Supporting Information

Dynamic supramacromolecular self-assembly: deformable polymer fabricated nanostructures through host-controlled approach

Qiang Yan, Jinying Yuan*, Yan Kang, Yingwu Yin

Contents

I. Experimental Section

II. Characterization

III. Further Discussion

IV. Schemes, Figures, and Tables

V. References

I. Experimental Section

Materials. Ethyl cellulose (EC, $M_{n,GPC}$ = 23000, the degree of ethyl substitution is 2.3) was obtained from LuZhou North Chemical Center and was dried at 90 ^{o}C for 24 h under vacuum before use. ε-Caprolactone (CL, Acros, 98%) was purified with CaH_2 by vacuum distillation in a nitrogen atmosphere. Methoxy poly(ethylene glycols)s (PEO) with M_n = 0.75K, 1.1K, 2K (i.e. $mPEO_{16}$, $mPEO_{24}$, $mPEO_{45}$) were dried by azeotropic distillation in the presence of toluene. Tin 2-ethylhexanoate (Sn(Oct)$_2$, Aldrich, 99%) was distilled under reduced pressure before use. Maleic anhydridie (MAh, Acros, 99%) was recrystallized from anhydrous chloroform free of ethanol. Dicyclohexylcarbodiimide (DCC, Alfa Aesar, 99%) and 4-dimethylaminopyridine (DMAP, Alfa Aesar, 99%) were used as received. Methanol was dried with molecular sieves type 4A before use. Methylene chloride (CH_2Cl_2), chloroform ($CHCl_3$), xylene, toluene, diethyl ether, and tetrahydrofuran (THF) were dried over CaH_2 and distilled before use.

Synthesis (the synthetic route shown in Scheme S1)**.**

Synthesis of EC-gPCL$_{10}$ Copolymer via Ring-Opening Polymerization (ROP). A typical polymerization procedure was shown as follows: EC (0.650 g, containing 2.03 mmol active hydroxyl groups) was dissolved in 15 mL of freshly anhydrous xylene in dried polymerization tube. CL (2.546 g, 22.3 mmol), a catalytic amount of Sn(Oct)$_2$, and a magnetic stirring bar were added into the polymerization tube. The tube was then connected to a Schlenk line, where exhausting-refilling processes were repeated 3 times. The tube was immersed into an oil bath at 120 ^{o}C under nitrogen atmosphere with vigorous stirring for 24 h. After cooling to room temperature, the resultant was dissolved in chloroform and precipitated twice with methanol to afford the purified graft copolymer. The purified copolymer was dried in a vacuum oven until constant weight. (Yield: 91%)

$M_{n,GPC}$ = 136100 g/mol, M_w/M_n = 1.24.

IR (KBr, cm^{-1}): 3460~3610 (ν_{O-H}), 2946 and 2886 (ν_{C-H}), and 1730 ($\nu_{C=O}$).

^{1}H NMR (CDCl$_3$, δ, ppm): 4.06 (t, -OC**H$_2$**CH$_2$CH$_2$CH$_2$CH$_2$COO-), 3.63 (t, terminal C**H$_2$**O), 3.06~3.82 (proton in EC backbone), 2.30 (t, -OCH$_2$CH$_2$CH$_2$CH$_2$C**H$_2$**COO-), 1.63 (m, -OCH$_2$C**H$_2$**CH$_2$C**H$_2$**CH$_2$COO-), 1.36 (m, -OCH$_2$CH$_2$C**H$_2$**CH$_2$CH$_2$COO-), 1.14 (s, -OCH$_2$C**H$_3$** on EC).

^{13}C NMR (CDCl$_3$, δ, ppm): 173.5 (-OCH$_2$CH$_2$CH$_2$CH$_2$CH$_2$**C**OO- in PCL), 71.2 (-O**C**H$_2$CH$_3$ in EC backbone), 64.3 (-O**C**H$_2$CH$_2$CH$_2$CH$_2$CH$_2$COO-), 34.4 (-OCH$_2$CH$_2$CH$_2$CH$_2$**C**H$_2$COO-), 31.0 (-OCH$_2$**C**H$_3$), 28.2 (-OCH$_2$**C**H$_2$CH$_2$CH$_2$CH$_2$COO-), 25.6 (-OCH$_2$CH$_2$CH$_2$**C**H$_2$CH$_2$COO-), 24.4 (-OCH$_2$CH$_2$**C**H$_2$CH$_2$CH$_2$COO-).

Synthesis of Carboxyl-Terminated mPEOs (mPEO-COOH). A typical example is given below. The mPEO2K (mPEO$_{45}$, 4.402 g, 4.00 mmol) and MAh (0.412 g, 4.20 mmol) were dissolved in 40 mL of anhydrous toluene, and the reaction was carried out at 70 ^{o}C for 16 h under vigorous stirring. The solvent was evaporated completely using a rotary evaporator. The residue was dissolved in CH_2Cl_2 and precipitated in diethyl ether and iced methanol to remove excessive MAh. The purified product was dried in vacuum until constant weight. (Yield: 87%)

$M_{n,GPC}$ = 2090 g/mol, M_w/M_n = 1.04.

IR (KBr, cm^{-1}): 3015 ($v_{C=C-H}$), 2882 (v_{C-H}), 1732 ($v_{C=O}$ in –COO–), 1646 ($v_{C=O}$ in –COOH), and 1150 (v_{C-O-C} in PEO).

^{1}H NMR (CDCl$_3$, δ, ppm): 6.31 (q, -C**H**=C**H**-), 3.64 (s, -C**H$_2$**C**H$_2$**O-), 3.37 (s, -OC**H$_3$**).

Synthesis of Comb-Copolymer EC-g-PCL$_{10}$-b-PEO$_x$ (x = 17, 24, and 45) via Efficient Coupling Reaction. A typical example was as follows. The EC-*g*-PCL$_{10}$ (1.020 g, 9.72 μmmol and containing active ended-hydroxyl groups 0.690 mmol), mPEO$_{45}$-COOH (0.985 g, 0.828mmol), DCC (0.175 g, 0.850 mmol), and DMAP (36.6 mg, 0.300 mmol) were dissolved in 20 mL of anhydrous CH$_2$Cl$_2$, and the reaction was performed at room temperature for 24 h under nitrogen atmosphere. The reaction byproduct dicyclohexylcarbodiurea was removed by filtration, and the filtered solution was evaporated to dryness. To remove the excessive mPEO$_{46}$-COOH, the solid was dissolved in CHCl$_3$, and the solution was extracted with a diluted HCl solution (pH = 5.0), followed by water, and then dried over anhydrous Na$_2$SO$_4$. After dried treatment the resultant was dialysis twice to purify and then precipitating from diethyl ether. (Yield: 94%)

$M_{n,GPC}$ = 327800 g/mol, M_w/M_n = 1.22.

IR (KBr, cm^{-1}): 3018 ($v_{C=C-H}$), 2920 (v_{C-H}), 1730 ($v_{C=O}$ in PCL), and 1147 (v_{C-O-C} in PEO).

^{1}H NMR (CDCl$_3$, δ, ppm): 6.30 (q, weak, -C**H**=C**H**-), 4.06 (t, -OC**H$_2$**CH$_2$CH$_2$CH$_2$CH$_2$COO-), 3.64 (s, -C**H$_2$**C**H$_2$**O-), 3.12~3.82 (proton in EC backbone), 2.30 (t, -OCH$_2$CH$_2$CH$_2$CH$_2$C**H$_2$**COO-), 1.63 (m, -OCH$_2$C**H$_2$**CH$_2$C**H$_2$**CH$_2$COO-), 1.36 (m, -OCH$_2$CH$_2$C**H$_2$**CH$_2$CH$_2$COO-), 1.14 (s, -OCH$_2$C**H$_3$** on EC).

^{13}C NMR (CDCl$_3$, δ, ppm): 173.9 (-OCH$_2$CH$_2$CH$_2$CH$_2$CH$_2$**C**OO- in PCL), 70.1 (-O**C**H$_2$**C**H$_2$- in PEO), 64.3 (-O**C**H$_2$CH$_2$CH$_2$CH$_2$CH$_2$COO-), 34.4 (-OCH$_2$CH$_2$CH$_2$CH$_2$**C**H$_2$COO-), 28.2 (-OCH$_2$**C**H$_2$CH$_2$CH$_2$CH$_2$COO-), 25.6 (-OCH$_2$CH$_2$CH$_2$**C**H$_2$CH$_2$COO-), 24.4 (-OCH$_2$CH$_2$**C**H$_2$CH$_2$CH$_2$COO-).

Preparation of Copolymer Self-Assemblies. In order to prepare micellar aggregates, copolymer **1** with different molars was dissolved in THF, which is a common solvent for both PCL and PEO blocks. Subsequently, deionized water was added to the polymer/THF solutions at a rate of 0.2 mL/h with vigorous stirring using a microsyringe. The resulting colloidal solutions were placed in dialysis bags and dialyzed against distilled water to remove the THF for subsequent studies.

Preparation of Dynamic Supramacromolecular Self-Assemblies. Continuously adding α-CD to the given micellar solution (1.50 × 10^{-6} M) rendered the concentration of α-CD in the binary polymer-α-CD solution to change at a wide range from 1.0 × 10^{-4} M to 9.7 × 10^{-3} M. The obtained new assembly solutions were dialyzed to remove unassembled host molecules for characterization. For the ternary system polymer-α-CD-phenol, we also continuously introduced competitive guest phenols (at same concentration range) to the polymer-α-CD solution and then dialyzed to remove dissociative phenols and α-CD/phenol complexes for *in-situ* observation.

II. Characterization

Fourier Transform Infrared Spectroscopy (FT-IR). The absorption spectra were recorded on a AVATAR 360 ESP FT-IR spectrometer and the results were collected at 30 scans with a spectral resolution of 1 cm^{-1}.

Nuclear Magnetic Resonance (NMR). ^{1}H NMR and ^{13}C NMR spectra for the copolymer structural analysis were obtained from a JEOL JNM-ECA300 spectrometer with CDCl$_3$ as the solvent. 1D-NMR and 2D-^{1}H-^{1}H COSY spectra for the characterization of dynamic host-guest interactions in the binary system polymer-α-CD and ternary system polymer-α-CD-phenol were obtained from JEOL JNM-ECA600 spectrometer with d$_6$-DMSO as a solvent. The chemical shifts were relative to tetramethylsilane at $\delta = 0$ ppm for protons.

Gel Permeation Chromatography (GPC). The molecular weight (M.W.) and molecular weight distribution (PDI) were measured on a Viscotek TDA 302 gel permeation chromatograph equipped with two columns (GMHHR-H and M Mixed Bed). THF was used as the eluent at a flow rate of 1 mL/min at 30 ºC. A series of low polydispersity polystyrene standards were employed for the GPC calibration.

Turbidity Measurements. The optical transmittance of copolymer solutions were acquired on a UV 2100 UV-visible spectrophotometer (Shimadzu, Japan) at a wavelength of 550 nm using a cuvette. The critical micelle concentration (CMC) of EC-*g*-PCL$_{10}$-*b*-PEO$_x$ (x = 17, 24, and 45) was determined from the turbidity changes at different copolymer concentrations in aqueous media. In addition, the dynamic self-assembly transition can also reflect on the turbidity measurements.

Fluorescence Spectroscopy. To further support the turbidity results, we used a pyrene probe to monitor the fluorescence changes at different solution conditions. Fluorescence spectra were recorded by a Perkin-Elmer LS55 spectrofluorometer. The slit widths were set at 5.0 nm for both the excitation and the emission. A calculated volume of pyrene solution in acetone was added to a volumetric flask, followed by removing the acetone under reduced pressure. The aqueous solutions of copolymer **1** at different concentrations then poured into volumetric flasks, pyrene concentration was fixed at 5×10^{-7} M in all cases. The characteristic feature of pyrene excitation spectra, which undergoes a shift from 332 to 338 upon pyrene partition into a micellar hydrophobic core, was employed to determine the CMC of EC-*g*-PCL$_{10}$-*b*-PEO$_x$ (x = 17, 24, and 45).

Laser Light Scattering. A commercial spectrometer (ALV/DLS/SLS-5022F) equipped with a multi-tau digital time correlator (ALV5000) and a 22 mW He-Ne laser (λ_0 = 632 nm) as the light source was used. In dynamic light scattering (DLS) experiments, scattering light was collected at a fixed angle of 90º for duration of ~10 min. Average radius $\langle R_h \rangle$ and particle size distributions $\langle f_h \rangle$ were computed using cumulants analysis and CONTIN routines. In static light scattering, we can obtain the apparent weight-average molar mass $\langle M_{w, \text{app}} \rangle$ and gyration radius $\langle R_g \rangle$ of assemblies from the angular dependence of the excess absolute scattering intensity, known as Rayleigh ratio $R_{vv}(q)$, as

$$\frac{KC}{R_{vv}(q)} \approx \frac{1}{M_w}(1 + \frac{1}{3} < R_g^{~2} > q^2) + 2A_2C$$

in which $K = 4\pi^2 n^2 (dn/dC)^2/(N_A \lambda_0^4)$ and q = $(4\pi n/\lambda_0)sin(\theta/2)$ with N_A, dn/dC, n, and λ_0 being the Avogrdro number, the specific refractive index increment, the solvent refractive index, and the

wavelength of laser light in a vacuum, respectively; and A_2 is the second virial coefficient.

Transmission Electronic Microscopy (TEM). The aggregate morphologies and reversible polymer nanostructures were visualized with a JEOL JEM-2010 TEM at an accelerating voltage of 120 kV. A small drop from the copolymer assemblies solutions was deposited onto carbon-coated copper grid. Before observation, the excess of aqueous solution was wiped off with filter paper, and the grid was dried under vacuum for 24 h.

Atomic Force Microscopy (AFM). AFM observations were conducted on a SPM-9500J3 tapping-mode atom force microscope (Shimadzu, Japan) and the assemblies samples preparation was similar to that for TEM, but newly cleaved fresh mica surface was used as the substrate.

X-ray diffraction (XRD). The crystalline patterns of copolymer assemblies were obtained at room temperature upon a Cu Kα radiation source using a Bruker AXSD8 Advance X-ray diffractometer (Bruker, Germany). The supplied voltage and current were set to 40 kV and 120 mA. Samples were exposed at a scanning rate of $2\theta = 4°$/min between 2θ values ranging from 5° to 60°.

III. Further Discussion

Preparation of EC-g-PCL₁₀ Copolymer via ROP. The graft polymerization of ε-CL with EC was carried out in the presence of Sn(Oct)₂ as a metal catalyst and xylene as a solvent to afford the EC-*g*-PCL copolymer via ROP.[1] Compared to cellulose, EC possesses good solubility in common organic solvents such as choloroform, THF, xylene, etc. Therefore, a homogeneous ROP reaction of ε-CL was successfully performed on the EC backbone in xylene because EC, ε-CL, and EC-*g*-PCL could be dissolved in xylene.[2] The FT-IR spectrum of EC-*g*-PCL copolymer is shown in Figure S1. The wide peak at 3180—3580 cm⁻¹ was the absorption band of the hydroxyl group on the periphery of graft copolymer (Figure S1b). As compared to the IR spectrum of pure EC (Figure S1a), the absorption of the hydroxyl group was decreased owing to polymerization, and a new absorption band at 1730 cm⁻¹ assigned to the carbonyl band of PCL could be detected. The major resonance peaks of ¹H NMR spectrum a—d were attributed to PCL (Figure S2a), and the methylene proton signal (a', δ = 3.63) indicated that PCL was terminated by hydroxyl groups. In addition, the ¹³C NMR spectrum of EC-*g*-PCL with assignment showed the typical signals of the PCL at δ = 173.5, 64.3, 34.4, 28.2, 25.6, and 24.4 ppm (Figure S3a). The average polymerization degree of ε-CL on every glucose unit of the EC backbone was calculated from GPC data.

Preparation of Comb-Copolymer EC-g-PCL₁₀-b-PEOₓ (x = 17, 24, and 45). The mPEO-COOHs used in the following coupling reaction were synthesized by reaction of mPEOs with MAh. The FT-IR spectrum showed the characteristic absorption band of ester carbonyl at v = 1732 cm⁻¹ and acid carbonyl at v = 1646 cm⁻¹, which indicated that the product was synthesized successfully. The coupling reaction of EC-*g*-PCL₁₀ with a slight excess of mPEO-COOH was carried out at room temperature in the presence of DCC and DMAP. As shown in Figure S1c, the intensity of the C—H stretching band of PEO at 2920 cm⁻¹ highly increased and the acid carbonyl absorption band at 1646 cm⁻¹ decreased dramatically, which suggested that mPEO-COOH was coupled with the PCL block.[3] In addition, the new absorption at 1147 cm⁻¹ ascribed to C—O—C resonance of PEO segments indicates the high coupling efficiency. As compared to the ¹H NMR spectrum of the copolymer EC-*g*-PCL in Figure S2a, new signal (g, δ = 3.64 ppm) assigned to methylene in PEO segments could be observed in Figure S2b. Additionally, it is notable that the quadruplex coupled peaks of ethylene on the linker (h, δ = 6.30 ppm, $J_{-HC=CH-}$ = 10 Hz), indicating the successful coupling. Similarly, the new peak at δ = 70.1 ppm in ¹³C NMR spectrum of EC-*g*-PCL-*b*-PEO ascribed to methylene carbon atom in PEO segments proved aforementioned results (Figure S3b). The compositions of these EC-*g*-PCL-*b*-PEOₓ (x = 17, 24, and 45) comb-copolymers could be obtained through GPC data (Table S1).

The CMC Measurements of Comb-Copolymer EC-g-PCL₁₀-b-PEOₓ (x = 17, 24, and 45). The optical transmittance measurements exhibited the CMC value of EC-*g*-PCL₁₀-*b*-PEOₓ (x = 17, 24, and 45) copolymers through the turbidity change (Figure S4). With the increase of PEO segments, the CMC of copolymer gradually reduced from 1.66×10^{-5} M to 1.42×10^{-6} M. Fluorescence detection using pyrene as a probe also illustrated corresponding CMC results (Figure S5). We chose EC-*g*-PCL₁₀-*b*-PEO₄₅ (copolymer **1**) to carry out subsequent experiments. Because its CMC value was a minimum at the concentration 1.46×10^{-6} M and its w_{EO} (~0.62) was closed to the threshold of morphological transition.

DLS Measurements for Dynamic Supramacromolecular Self-Assemblies.

For the copolymer **1**, DLS revealed that their micellar aggregates maintained almost on a constant R_h (12─18 nm) at different concentrations above the CMC value (Figure S6). The $M_{w, app}$s of these aggregates were calculated from 2.3×10^6 g/mol to 4.1×10^6 g/mol, and the aggregated number ($N_{agg} = M_{w, app}/M_w$) was from 7 to 13, implying that the morphology and composition of these micellar aggregates could not change along with the copolymer concentration. These results were demonstrated that simplex copolymer assemblies exhibited a single phase state and had not the phase transition behavior due to its fixed amphiphilicity (w_{EO}).

However, surprisingly, when a host molecule α-CD added in the copolymer solution, a series of dynamic supramacromolecular self-assembly transitions took place (Figure S7). In the presence of 3.6×10^{-4} M α-CDs, the R_h of these aggregates increased abruptly to about 51 nm and a spot of smaller aggregates coexisted (5 nm< R_h < 20 nm). The wide size distribution, ⟨f_h⟩, demonstrated that the assemblies adopted on an intellectual metastable phase state. Sequential increasing α-CDs to 2.3×10^{-3} M, a type of new aggregates were detected and its R_h was approximately 69 nm. The narrow size distribution indicated that these assemblies had almost uniform geometrical shape and global morphology, that is, vesicles. It is unimaginable that these vesicles could further transform into a new superstructure with giant radius (> 400 nm) and much broader size distribution when the α-CD concentration is up to 8.7×10^{-3} M. To dynamically monitor the size variation of supramacromolecular self-assemblies, we use DLS to record the R_h changes at a gradient α-CD concentration from 0 M to 9.5×10^{-3} M (Figure S8). We can observe that in the absence of α-CD the copolymer assembled into spherical micelles. Adding host species gradually, the size of these assemblies enlarged three-fold than that of origins and the equilibrium range of these assemblies range is narrow from 2.4×10^{-4} M to 8.8×10^{-4} M; moreover, the $M_{w, app}$ and N_{agg} changed to 1.9×10^7 g/mol and 58, respectively. These abrupt increments on $M_{w, app}$ and N_{agg} confirmed that the cylindrical nanostructure had been formed and it stood on a metastable phase state. In contrast, as continuously adding α-CDs, the R_h of polysomes went up whereas the $M_{w, app}$ and N_{agg} had a slight decrease ($M_{w, app} = 1.2 \times 10^7$ g/mol and $N_{agg} = 38$), which demonstrated that the assemblies tended to a hollow and lower-curvature vesicular morphology. With the addition of α-CDs the size of the assemblies had a tremendous jump and the $M_{w, app}$ was abruptly excess of 10^8 g/mol, which suggested that vesicular shapes were unable to keep the stability of assemblies. The huge R_h and statistic-distribution-free data illustrated the planar and irregular sheetlike superstructure formed.

For the opposite process, an invertible "top-down" disassembly was observed by *in-situ* DLS characterization (Figure S10). In the terms of adding competitive guest, the polymer-α-CD-phenol ternary system had been established. Controlling over the quantity of phenols, above diversified supramacromolecular assemblies were able to disassociate α-CDs from the copolymer side chains stepwise, inducing a hierarchical self-disassembly process from sheet through vesicle to cylinder and back to initial global micellar structure. However, it is notable that the vesicles (size ~90 nm) and cylinders (size ~70 nm) are both smaller than that of initial assemblies. We considered that vesicular and cylindrical geometries are in the transition phase whereas micellar and sheetlike geometries are in the stable state, therefore, for the dynamic assembly or disassembly process the metastable phase is unable to return to initial morphology completely.

AFM Images for Further Proving the Dynamic Supramacromolecular Self-Assembly Transition.

From the AFM height images as shown in Figure S9, we can see the dynamic assembly transition again from micelles through cylinders to vesicles and further to sheet superstructure based on different α-CD concentrations. Notably, the wall thickness of the sheets is around 8 nm close to the width of single macromolecule. It is suggested that the plane possesses only one molecular layer like sandwich structure. The bottom and upper layers are both composed of dense PEO/PCL polyrotaxanes, which are polymer and α-CD self-threading complexes. The middle layer is composed of hydrophobic EC backbone.

1D-NMR and 2D-^{1}H-^{1}H COSY NMR Spectra for the Dynamic Host-Guest Interactions. To further validate the mechanism of dynamic host-guest interactions inducing the self-assembly evolution in manuscript, we utilized the 1D-NMR and 2D-^{1}H-^{1}H COSY NMR spectra to monitor the proton signal change between α-CD and copolymer.[4] As expected, with the assembly transition from cylinders through vesicles to sheets, the resonance peaks of PEO (δ = 3.64) and PCL (δ = 4.06) are gradually depressed. In contrast, the intensity of α-CD proton signals (δ = 3.67~3.80) rises up increasingly via 1D-NMR (Figure S11). These results demonstrate that α-CD molecules are hierarchically seized into the PEO and PCL segments, which indirectly elucidates the dynamic feature of this host-guest interaction.[4] Moreover, the proton relationship between α-CD and copolymers by 2D-NMR can dictate the point.[5] For example, wormlike micelles showed weak correlated peaks between internal H-3 of α-CD and central proton of ethylene oxide (EO) unit (Figure S12a, red circles), indicative of less α-CD/PEO threading complexes, that is, per PEO graft having 1~2 host molecules averagely by calculated. In the case of vesicular aggregates, more intensive and extended signals between EO unit and α-CD cavities (H-2, H-5 and H-6) are observed (Figure S12b, red circles), confirming that per PEO segments possess even more α-CDs (7~9). Most strikingly, the spectrum of sheetlike objects exhibited significant distinction (Figure S12c). The further enhancement of host-guest relevant signals indicates the formation of dense polyrotaxanes (red circles). It is notable that PCL side chains also involve in the threading association (blue circles). Meanwhile the intermolecular correlation of α-CDs is strengthened (green circles), which implies that these polyrotaxanes tend parallel alignment onto the skeleton of comb-copolymers. For the opposite hierarchical disassociation procedure, Figure S14 shows the resonance dynamic variation when competitive guest phenols remove α-CD away from copolymer chains step by step. As expected, from sheets through vesicles back to cylinders, the peaks of PEO (δ = 3.64) and PCL (δ = 4.06) are clearly enhanced. In contrast, the intensity of α-CD proton signals (δ = 3.67~3.80) reduces slowly, indicating the host-guest interplay depression and proving the hierarchical disassembly phenomenon.

XRD Measurements for the Structure of Supramacromolecular Self-Assemblies. The XRD results could consolidate above mechanism and revealed the fine structure of different assemblies (Figure S13). In the absence of α-CD, copolymer **1** showed intensive diffraction peaks at 2θ = 19.1º and 23.6º, which are uniform with PEO and PCL double crystalline patterns.[6] However, once adding α-CD species to induce the formation of vesicular or sheetlike structures, the PCL and PEO conventional crystallinity is dramatically suppressive, and a diagnostic diffraction peak at 2θ = 19.8º for the channel structure of α-CD polyrotaxanes quite strengthening.[7] It is demonstrated that the host molecules α-CD are indeed trapped onto the copolymer side chain from outer PEO blocks throughout to wholly PEO/PCL grafts hierarchically.

IV. Schemes, Figures, and Tables
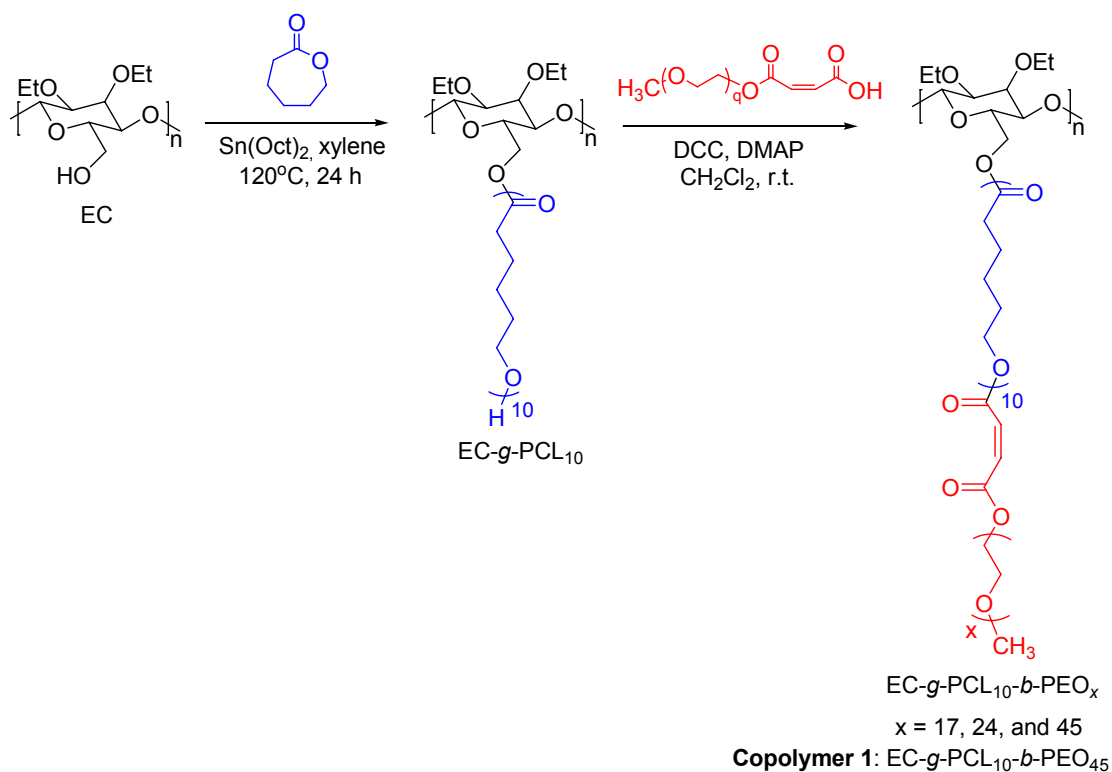
Scheme S1. Synthetic routes for the preparation of EC-g-PCL-b-PEO via a combination of ROP and efficient coupling reactions.
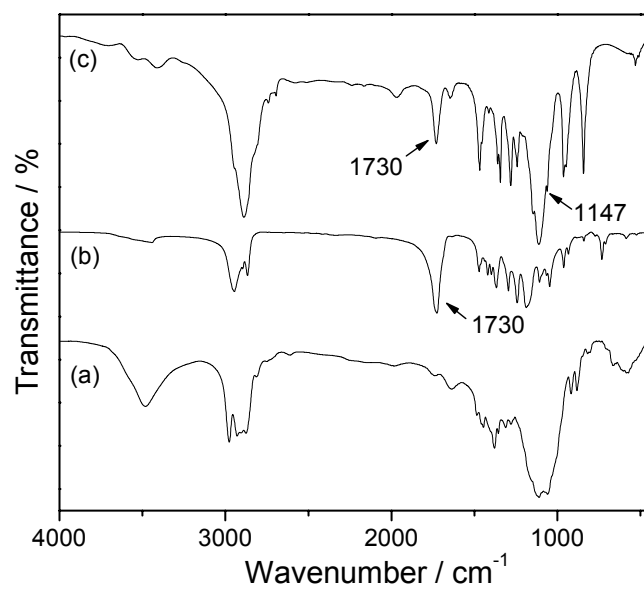
Figure S1. FT-IR spectra of (a) EC, b) EC-*g*-PCL, and c) EC-*g*-PCL-*b*-PEO.
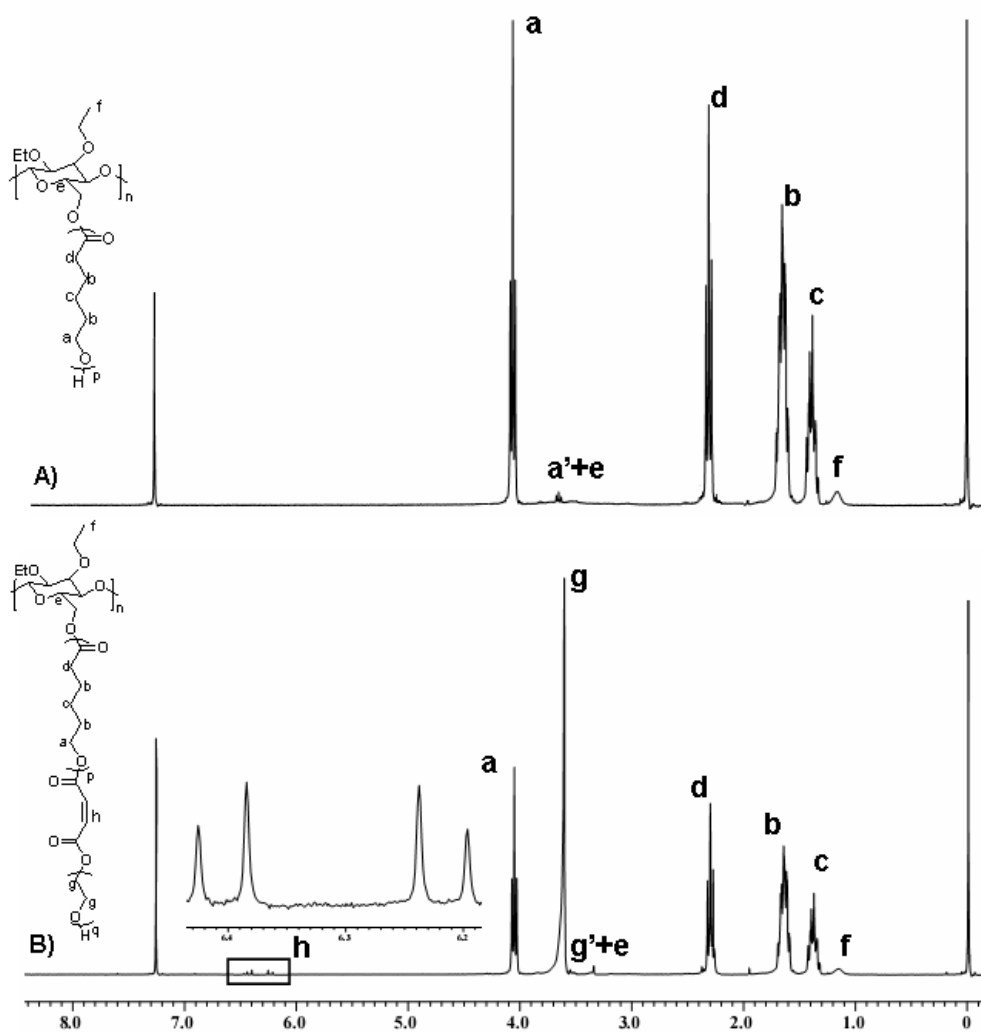
Figure S2. ^{1}H NMR spectra of a) EC-*g*-PCL and b) EC-*g*-PCL-*b*-PEO in CDCl$_3$.
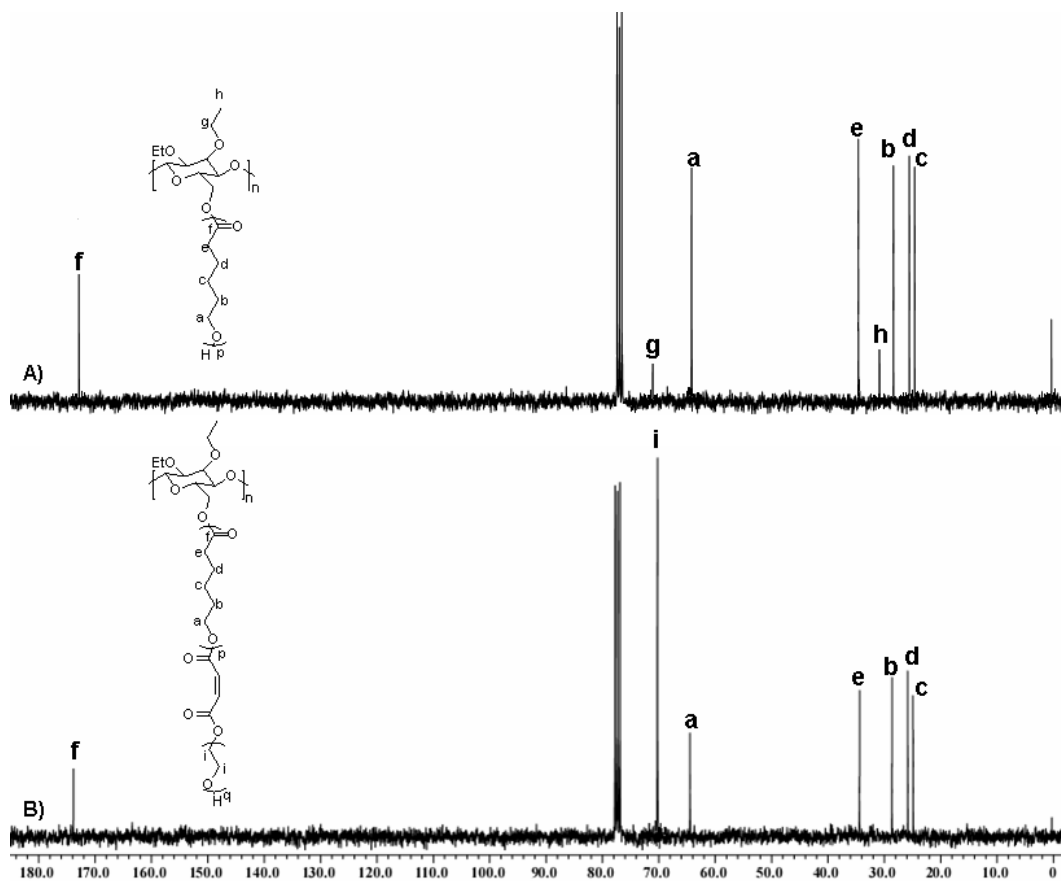
Figure S3. ^{13}C NMR spectra of a) EC-*g*-PCL and b) EC-*g*-PCL-*b*-PEO in CDCl$_3$.

Table S1. **Macromolecular Parameters of Comb-Copolymer EC-*g*-PCL-*b*-PEO via ROP and efficient coupling reaction.**

No.	Sample[a]	w_{EO} [b]	$M_{n,th}$[c] (kg/mol)	$M_{n,NMR}$[d] (kg/mol)	$M_{n,GPC}$[e] (kg/mol)	PDI[e]
1	EC-*g*-PCL$_{10}$-*b*-PEO$_{17}$	0.35	187.8	213.7	210.8	1.34
2	EC-*g*-PCL$_{10}$-*b*-PEO$_{24}$	0.47	217.5	248.1	232.9	1.29
3	EC-*g*-PCL$_{10}$-*b*-PEO$_{45}$ (**1**)	0.62	352.2	342.6	327.8	1.22

[a] The structures of samples are determined by $M_{n,NMR}$.
[b] w_{EO} is the weight fraction of PEO segments in copolymer
[c] $M_{n,th}$ is determined by the mass of final product.
[d] $M_{n,NMR}$ is determined by ^{1}H NMR spectroscopy.
[e] $M_{n,GPC}$ and PDI are determined by GPC analysis with polystyrene standards.
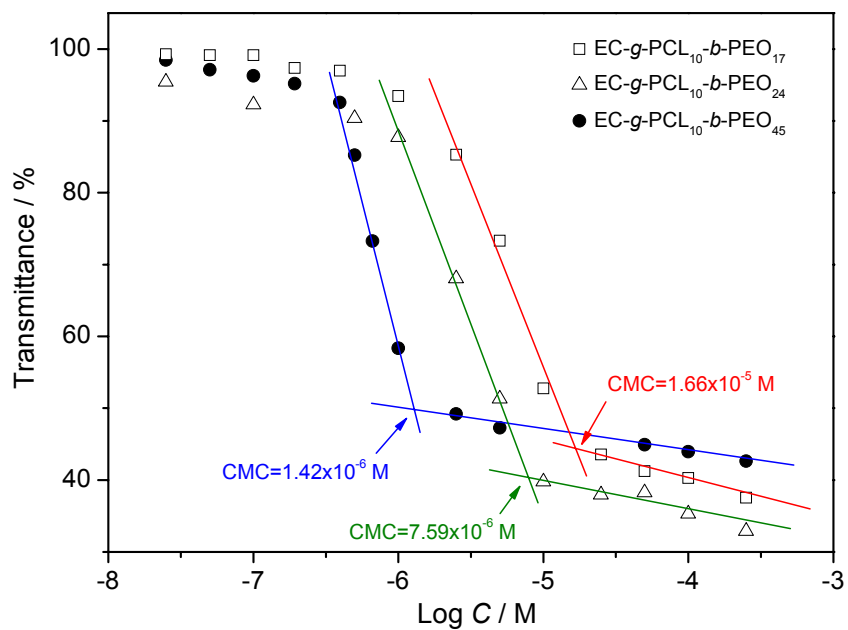
Figure S4. Plots of turbidity changes of comb-copolymers EC-*g*-PCL$_{10}$-*b*-PEO$_x$ (x = 17, 24, and 45) in aqueous solution at different concentration.
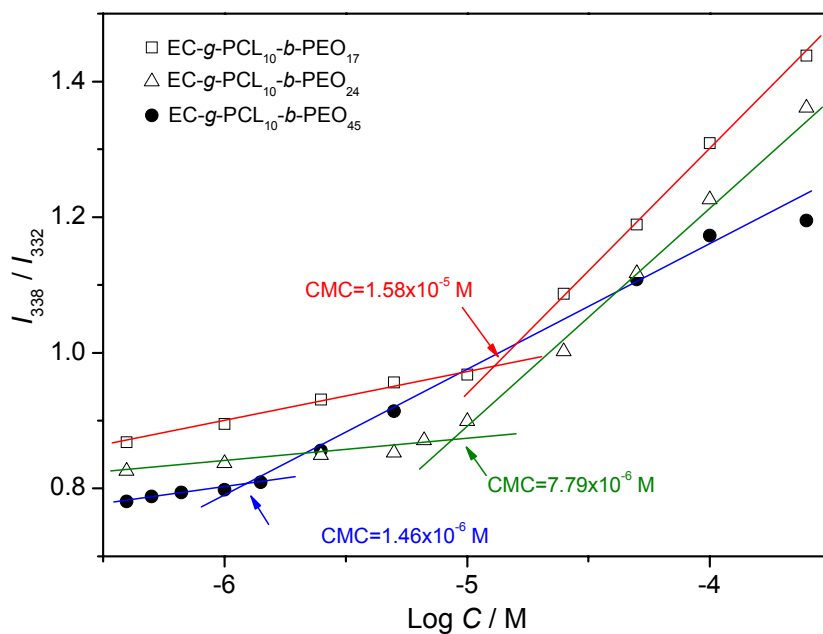
Figure S5. Plots of fluorescence intensity ratios (I_{338}/I_{332}) from pyrene excitation spectra as a function of the concentration of comb-copolymer EC-g-PCL$_{10}$-b-PEO$_x$ (x = 17, 24, and 45) in aqueous solution. Pyrene concentration was fixed at 5×10^{-7} M.
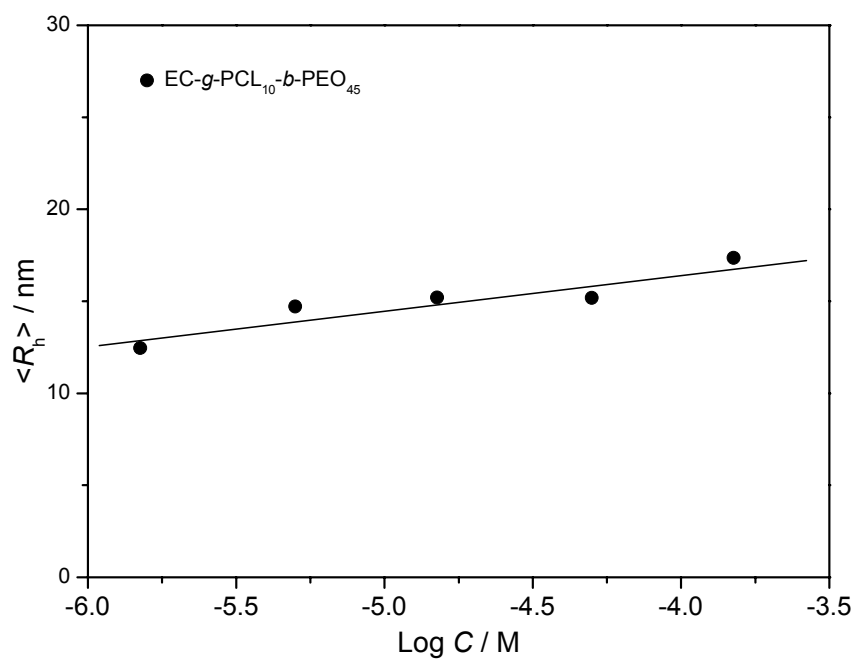
Figure S6. Variation of average hydrodynamic radius, $\langle R_\mathrm{h} \rangle$, as a function of pure copolymer **1** (EC-*g*-PCL$_{10}$-*b*-PEO$_{45}$) micellar assemblies with different concentrations. The data is collected at a fixed scattering light angle of 90º.
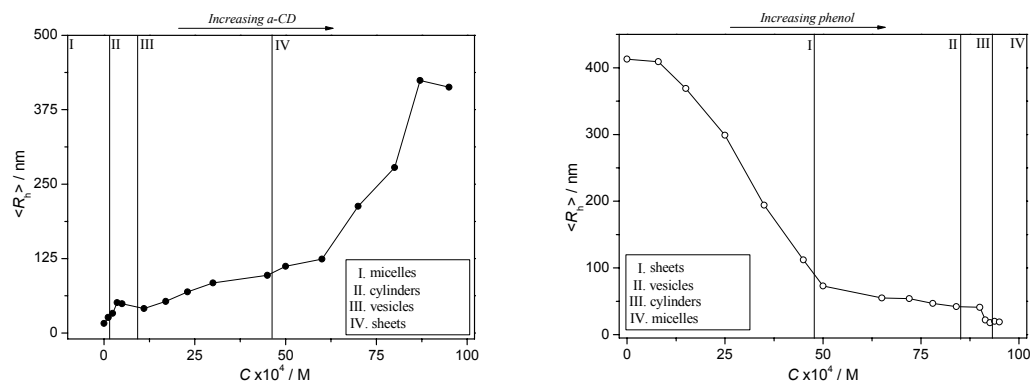
Figure S7. The size-variation curve of supramacromolecular self-assemblies and disassembly evolution upon dynamic increasing the host (left) or guest (right) concentration between 0 M and 9.5×10^{-3} M.
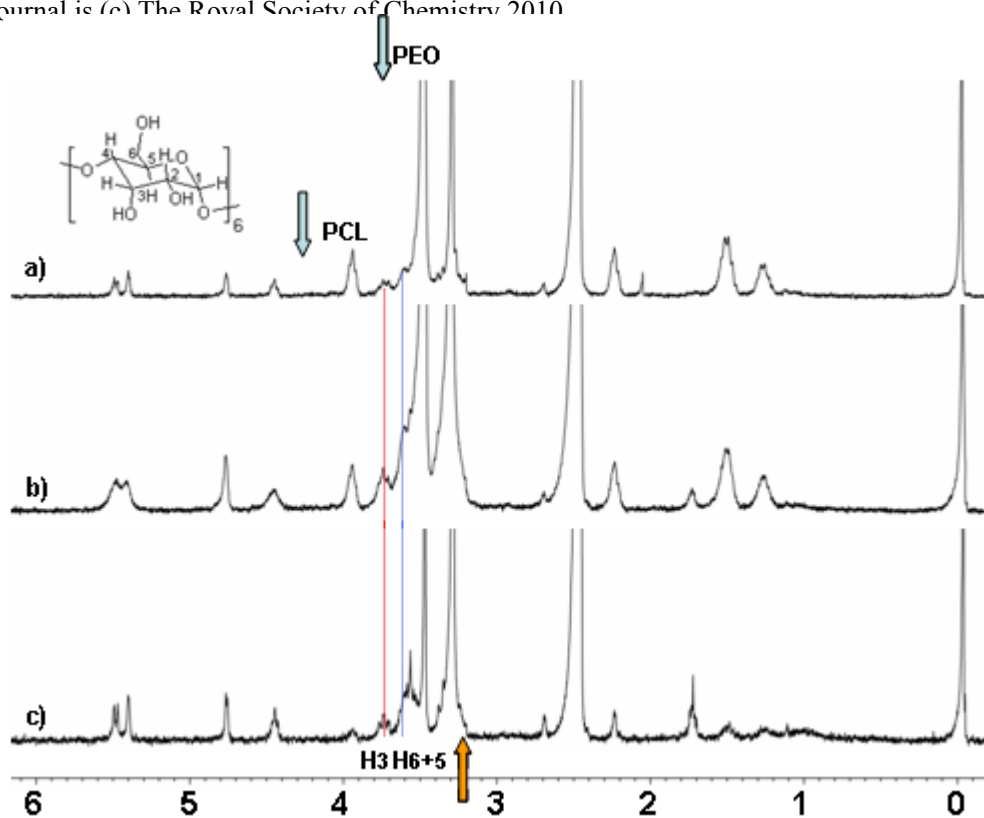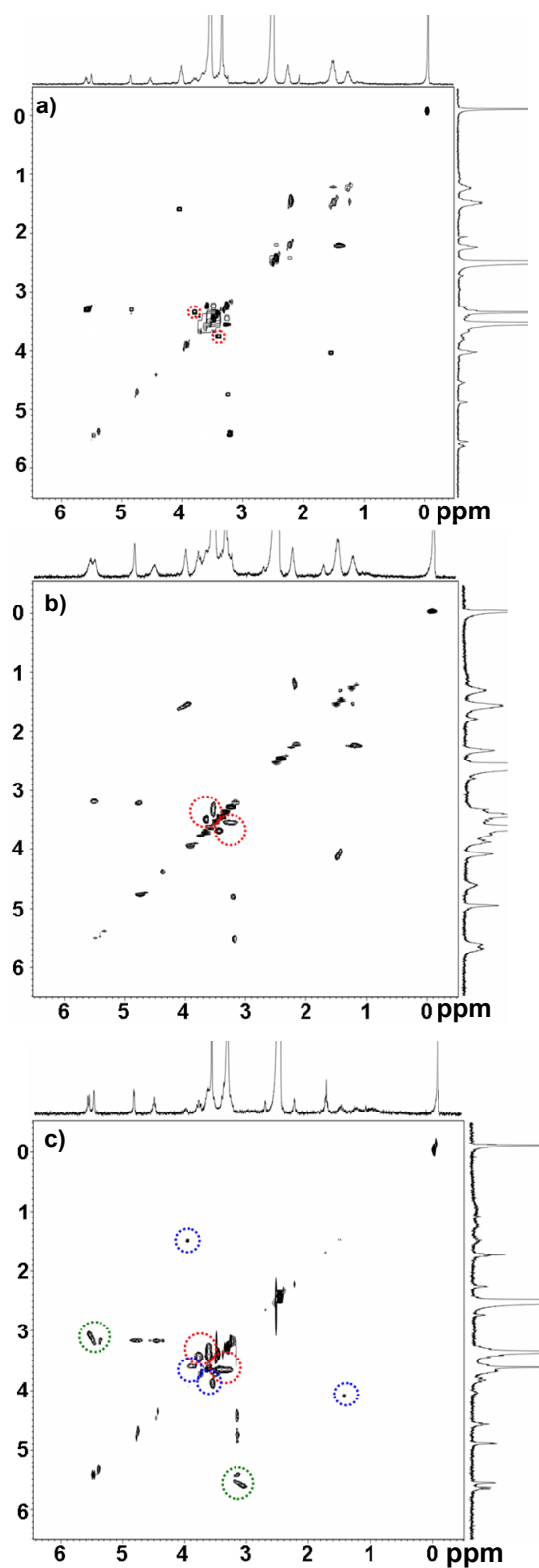
Figure S8. 1D-^{1}H NMR spectra of polymer-α-CD supramacromolecular assemblies with various α-CD concentration: a) cylinder phase (3.6×10^{-4} M α-CDs), b) vesicular phase (2.3×10^{-3} M α-CDs), and c) sheet superstructure phase (8.7×10^{-3} M α-CDs). All samples were characterized in d_6-DMSO.

Figure S9. 2D-^{1}H-^{1}H COSY NMR spectra of polymer-α-CD supramacromolecular assemblies with various α-CD concentration: a) cylinder phase (3.6×10^{-4} M α-CDs), b) vesicular phase (2.3×10^{-3} M α-CDs), and c) sheet superstructure phase (8.7×10^{-3} M α-CDs). All samples were characterized in d_6-DMSO.
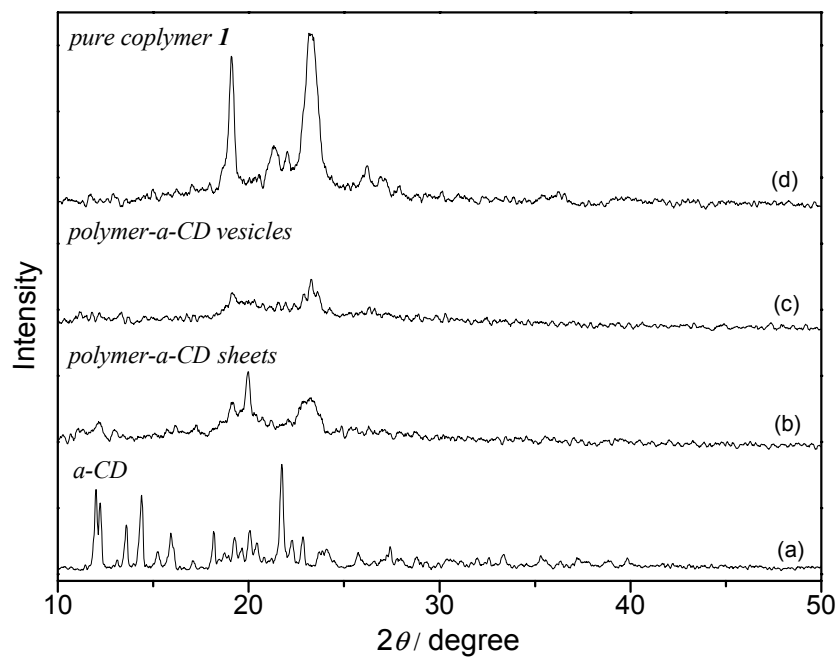
Figure S10. The crystalline behaviors comparison among α-CD, copolymer **1**, and supramacromolecular assembles: (a) α-CD powder, (b) sheets assemblies, (c) vesicles assemblies, and (d) copolymer **1** by XRD measurements.
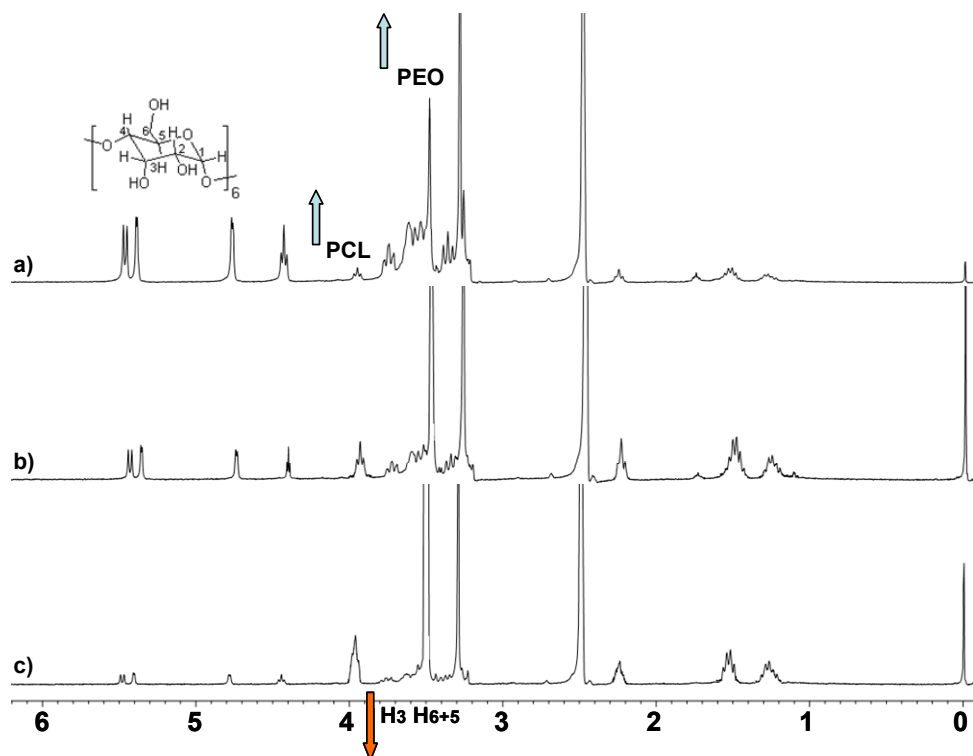
Figure S11. 1D-^{1}H NMR spectra of polymer-α-CD supramacromolecular assemblies with various phenol concentration: a) sheet superstructure phase (1.2×10^{-3} M phenols), b) vesicular phase ($4,7 \times 10^{-3}$ M phenols), and c) cylinder phase (8.2×10^{-3} M phenols). All samples were characterized in d_6-DMSO.

V. References

(1) (a) Ni, Q.; Yu, L. *J. Am. Chem. Soc.* **1998**, *120*, 1645-1646. (b) Albertsson, A.–C.; Varma, I. K. *Biomacromolecules* **2003**, *4*, 1466-1486.

(2) (a) Yan, Q.; Yuan, J. Y.; Zhang, F. B.; Sui, X. F.; Xie, X. M.; Yin, Y. W.; Wang, S. F.; Wei, Y. *Biomacromolecules* **2009**, *10*, 2033-2042. (b) Yuan, W. Z.; Yuan, J. Y.; Zhang, F. B.; Xie, X. M. *Biomacromolecules* **2007**, *8*, 1101-1108.

(3) Yuan, W. Z.; Yuan, J. Y.; Zhang, F. B.; Xie, X. M.; Pan, C. Y. *Macromolecules* **2007**, *40*, 9094-9012.

(4) Dong, H. Q.; Li, Y. Y.; Li, S. J.; Cai, J.; Zhuo, R. X.; Zhang, X. Z.; Liu, L. J. *Angew. Chem. Int. Ed.* **2008**, *47*, 5573-5576.

(5) (a) Inoue, Y.; Miyauchi, M.; Nakajima, H.; Takashima, Y.; Yamaguchi, H.; Harada, A. *J. Am. Chem. Soc.* **2006**, *128*, 8994-8995. (b) Inoue, Y.; Miyauchi, M.; Nakajima, H.; Takashima, Y.; Yamaguchi, H.; Harada, A. *Macromolecules* **2007**, *40*, 3256-3262.

(6) (a) Deng, M. X.; Chen, X. S.; Piao, L. G.; Zhang, X. F.; Dai, Z. L.; Jing, X. B. *J. Polym. Sci., Part A: Polym. Chem.* **2004**, *42*, 950-959. (b) He, C. L.; Sun, J.; Deng, C.; Zhao, T.; Deng, M. X.; Cheng, X. S.; Jing, X. B. *Biomacromolecules* **2004**, *5*, 2042-2047.

(7) (a) Rusa, C. C.; Fox, J.; Tonelli, A. E. *Macromolecules* **2003**, *36*, 2742-2747. (b) Lu, J.; Shin, I. D.; Nojima, S.; Tonellia, A. E. *Polymer* **2000**, *41*, 5871-5883.